ELSEVIER

Journal of Nuclear Materials 251 (1997) 72–76

journal of nuclear materials

Heat and mass transport in nanoscale phase transitions induced by collision cascades

A. Caro [a,*], M. Alurralde [b], R. Saliba [a], M. Caro [a]

[a] *Centro Atómico Bariloche, 8400 Bariloche, Argentina*
[b] *Centro Atómico Constituyentes, Libertador 8250, 1429 Buenos Aires, Argentina*

Abstract

Irradiation of materials with energetic particles produces changes in the microstructure that affect mechanical properties. In previous work we studied the thermal aspects of the quenching of collision cascades that involve nanoscale phase transitions between the solid and the liquid states of the target. In this work we present a rigorous treatment of these phenomena, including a detailed description of the Stefan problem in three dimensions and diffusion in thermal gradients. This approach is oriented to give a quantitative description of the influence of the primary knock-on spectrum on the microstructure short after the quenching of the heat spike. © 1997 Elsevier Science B.V.

1. Introduction

Irradiation of materials with energetic particles produces changes in many physical properties, in particular it alters the microstructure in such a way that it affects mechanical properties. The time scale involved in the evolution of the microstructure covers from the very early collisional stage (10^{-15} s) to slow diffusion processes spanning days or years.

In a series of previous work we have studied the thermal aspects of the quenching of collision cascades, that involve nanoscale phase transition between the solid and the liquid states of the target material. In this process, lasting a few picoseconds, very large thermal gradients as well as the solid–liquid interface produce thermodynamic forces driving intrinsic defects, impurities or solute elements towards aggregation or dissolution. Some of these effects, especially involving intrinsic defects, have microscopically been observed in molecular dynamics computer simulations, although a thermodynamic model for the general case is still missing.

A proper description with predictive power has to consider a series of physical properties that surely play a role, like equilibrium phase diagram, diffusion in solid and liquid phases, solidification kinetics, elastic, mechanical and thermal characteristics of the material, with particular emphasis on thermal conductivity and electron–phonon interaction. All together it represents a formidable challenge and we can say that today most of our knowledge relies on qualitative concepts with little, if any, predictive power.

The approach that we proposed in our previous work and that we extend here, tries to analyze to which extent usual thermodynamics is able to describe this process; the method we use is to link thermodynamic modeling to the results provided by molecular dynamics and experiments when available, trying to highlight the most important physical concepts involved. For this link to be realistic, all processes beyond thermodynamics, like momentum transport, shock waves and focusons have to play a minor role. Some of these points are discussed in detail in Refs. [1–3].

2. Results

We introduce now the ideas and approximations used in our liquid drop model (LDM) [1–3] to better understand

* Corresponding author. Tel.: +54-944 45 260; fax: +54-944 45 299; e-mail: caro@cab.cnea.edu.ar.

PII S0022-3115(97)00218-3

the contributions of the present work. In the binary collision approximation (BCA) the cascade develops inside a solid as a consequence of two body collisions [4]. An atom is set into motion if, as a consequence of a collision, it receives an energy larger than some cut-off, E_c. Similarly an atom no longer moves if its energy falls below E_c. A cascade ends when all atoms have energy below E_c. Additional parameters are the binding energy, E_b, which is lost every time an atom is displaced from its perfect lattice position and the parameters controlling the electronic losses. The energy balance is as follows: The total initial energy, i.e., the kinetic energy of the primary knock-on atom, E_{PKA}, is distributed between the inelastic collisions with the electrons, E_i, the kinetic energy given to secondary atoms, E_k, the kinetic energy below E_c given to atoms that are not displaced (this energy is called damage energy), E_D and the binding energies lost at each displacement, E_b. We have $E_{PKA} = E_i + E_D + E_k$.

As input of our LDM we use the output of the well known Marlowe BCA code [4], which contains the position and kinetic energy of all atoms set into motion during the collisional phase of the cascade. Since $E_k < E_{PKA}$, we apply a multiplicative factor which is discussed in detail in Ref. [1]. This kinetic energy is assumed to be transformed into thermal energy in a time of the order of one picosecond or less and then is transported by the heat equation. We showed that this approach gives results in full agreement with MD for cascade energies where both methods can be used. We applied it to different materials and PKA energies, and determine the life time, the volume of the melt and the ion mixing [2]. Also the intracascade contribution to radiation enhanced diffusion (RED) was evaluated [3].

Those works were based on a very simple assumption concerning the role of the interface in the heat transport and a later careful analysis showed that it may not be negligible [5]. Also, in our previous work we did not consider mass transport but only ion mixing, by just integrating a thermally activated process in the volume and lifetime of the heat spike.

In an attempt to interpret the thermal evolution of a heat spike using tools derived from near-to-equilibrium thermodynamics [5] we observed that as far as the system does not undergo a phase transition, linear irreversible thermodynamics apply and lattice transport can be described in terms of Fourier equations. However if the heat spike rises the temperature of the solid well above the melting temperature, our elementary approach (that neglected latent heat of melting) gave a poor description. The correct description should incorporate a treatment of the Stefan problem, that is, heat transport in presence of an interface. The general 3D case has no analytic solution, but a numerical algorithm to solve it has been recently proposed by Nochetto et al. [6–10]. We report here the first results of our implementation of these ideas.

Energy conservation together with Fourier law for heat flux leads to the following two-field equations:

$$\begin{cases} \dfrac{\partial u}{\partial t} + \nabla \cdot \boldsymbol{q} = 0 \\ \boldsymbol{q} = -\kappa(\theta)\nabla\theta \\ u(\theta) = \displaystyle\int_{\theta_{fus}}^{\theta} c(s)\,\mathrm{d}s + \lambda H(\theta - \theta_{fus}), \end{cases} \tag{1}$$

where u is the enthalpy, $\boldsymbol{q}$ is the heat flux, θ is the temperature, κ is the thermal conductivity, c is the heat capacity, H is the Heaviside function and λ is the latent heat of melting. Note that although θ is a function of u, $\theta = \beta(u)$, its inverse is not. Introducing the Kirchhoff transform $K = \kappa(\theta)$, defined as

$$K = \int_{\theta_{fus}}^{\theta} \kappa(s)\,\mathrm{d}s, \tag{2}$$

the original system of Eq. (1) becomes

$$\begin{cases} \dfrac{\partial u}{\partial t} - \nabla^2 K = 0 \\ u = \gamma(K), \end{cases} \tag{3}$$

where the function $u = \gamma(K)$ is obtained from the definition of the Kirchhoff transform and the enthalpy; u is a discontinuous function of K.

We skip here the details of the algorithms that allow this discontinuity to be dealt with and just say that we apply finite elements, implicit discretization to solve these equations. For a general reference to this method see Ref. [11].

As a test we solve a one dimensional temperature gradient on a three-dimensional rod, where both exact analytic solution and molecular dynamics results are available [5]. Fig. 1 shows the temperature profile at different times for a sample at uniform initial temperature above melting temperature T_m and with an end set at $T < T_m$ at $t = 0$. The discontinuous derivative of the temperature at T_m is a consequence of the non-zero heat of melting.

This description should account for the differences between the temperature profiles found in molecular dynamics and predicted by the heat equation, as reflected in fig. 1 in Ref. [5].

It is important to point out that in this analysis no mention is done to overheating and undercooling effects appearing in first order phase transitions. The reason is that on heating, the collisional disorder is such that no traces of the crystalline order in the core of the cascade remains, facilitating the nucleation of the liquid phase without overheating. On the other hand, on cooling, the liquid phase is surrounded by a perfect crystal, so there is no need of nucleation and growth of a germ of a crystallite. This hypothesis is supported by molecular dynamics re-

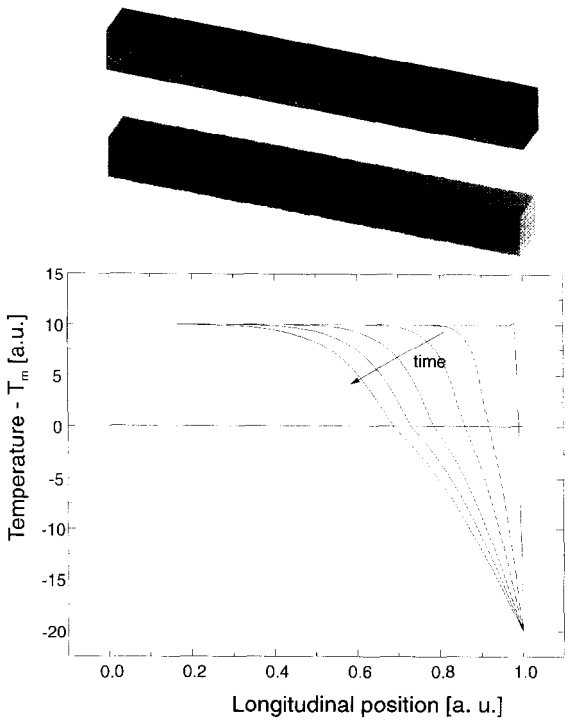

Fig. 1. Temperature profile at different times for a sample at uniform initial temperature above melting temperature T_m and with the left end set at $T < T_m$ at $t = 0$. Profiles shown at increasing times, as indicated by the arrow. Upper part, two snapshots of the sample used in the numerical treatment showing the grid and temperature profiles.

sults of heat spikes induced by collision cascades, where none of these effects is observed.

With a description of energy transport, the next step is mass transport. Here again, the first approximation is to assume that the Onsager relations [12–14] which are derived for small departures from equilibrium, are still valid in systems so far from equilibrium. For mass transport in presence of concentration and temperature gradients, these relations read

$$\begin{aligned} \boldsymbol{J} &= -D\nabla\rho + \frac{c_T \rho}{T^2}\nabla T \\ \frac{\partial\rho}{\partial t} &= -\nabla\cdot\boldsymbol{J} \end{aligned} \quad , \tag{4}$$

where $\boldsymbol{J}$ is the particle flux, D is the diffusion coefficient, ρ is the particle density, T is the temperature and c_T is the kinetic coefficient for the irreversible process linking thermal gradients to particle motion.

Most of these coefficients are unknown for the elements and the combination of elements of interest, in the temperature ranges created by heat spikes. Therefore in what follows we present a parametric study to determine the characteristics of the process and the first steps to determine some of them from molecular dynamics simulations.

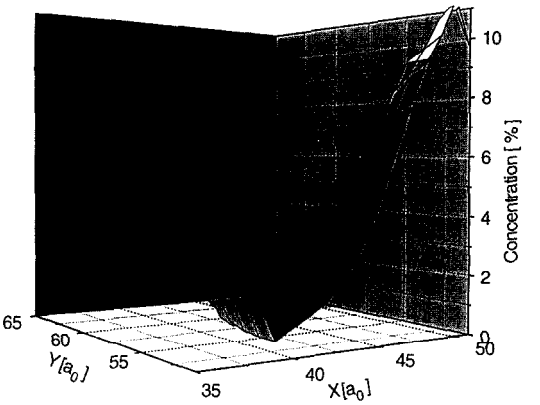

Fig. 2. Concentration profile for a system of initial uniform 2 at.% impurity content under the effects of an spherical Gaussian heat spike of 30 keV, in Ag. Negative thermal coupling coefficient $c_T = -10^4$ KÅ^2/s.

In Fig. 2 we show the concentration profile for a system of initial uniform 2 at.% Cu content in Ag under the effects of an spherical Gaussian heat spike of 30 keV of total energy and energy density corresponding to Ag. For this example, thermal conductivity is extracted from Ref. [5], diffusion coefficient from the hard sphere model of Protopapas et al. [15] and thermal coupling coefficient is chosen arbitrarily as $c_T = -10^4$ KÅ^2/s. Thermal conductivity and heat capacity are taken from the literature with their temperature dependence included in the calculation. Note that this work is a parametric study in terms of c_T, which is not available in the literature. The situation with negative coupling corresponds to precipitation, which should not be taken as the tendency to precipitation or segregation induced by thermodynamic forces derived from the phase diagram. In Fig. 3 we show equivalent results for

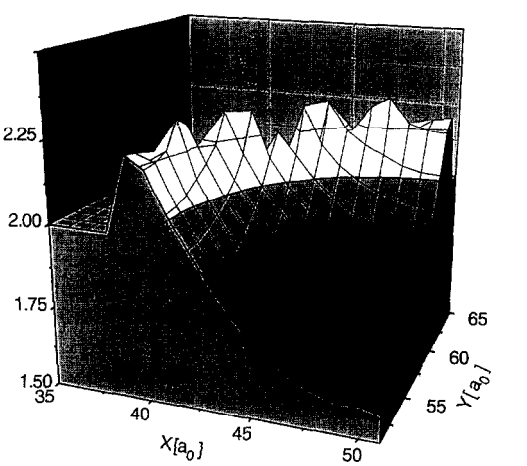

Fig. 3. As Fig. 2, for a positive $c_T = 10^3$ KÅ^2/s.

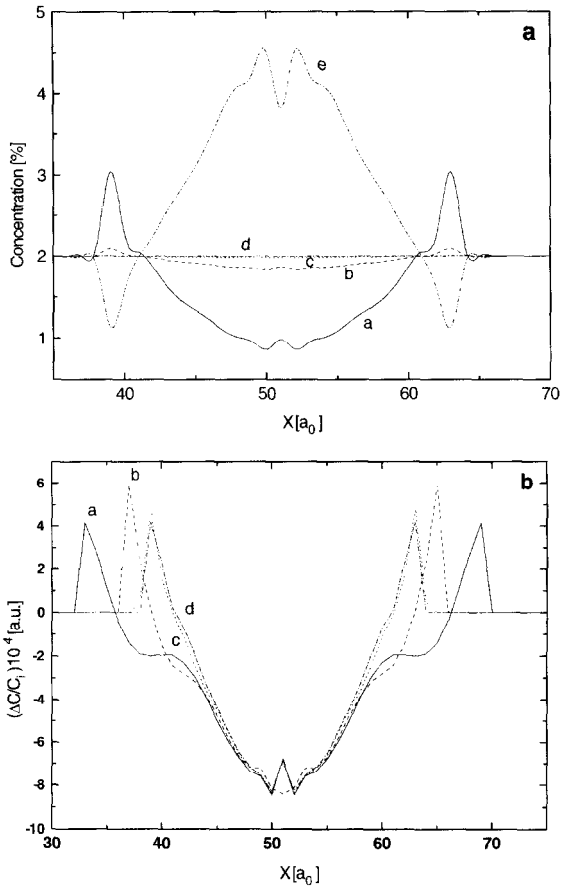

Fig. 4. (a) Sensitivity to c_T values: curve (a) $c_T = 10^4$, (b) $c_T = 10^3$, (c) $c_T = 10^2$, (d) $c_T = 10^1$ and (e) $c_T = -10^4$, in units of K Å^2/s. (b) Sensitivity to lattice temperature: curve (a) $T = 900$ K, (b) $T = 500$ K, (c) $T = 100$ K, (d) $T = 10$ K. Modeled material: Ag, $T_m = 1234$ K.

a positive $c_T = 10^3$ K Å^2/s, that would model the situation for ideal solid solutions. Fig. 4 shows the sensitivity to c_T values (Fig. 4a) and to lattice temperature (Fig. 4b).

In Figs. 5 and 6 we show results for real 10 and 500 keV in Ag as described in the binary collision approximation (Marlowe) and in the liquid drop model, containing a low concentration of solute Cu. Diffusion coefficient for Cu in Ag is taken from experimental results of Ref. [16] for the solid phase and from hard spheres model, Ref. [15] for the liquid phase. Coupling coefficient is $c_T = 10^4$ K Å^2/s in both cases. Figs. 5 and 6 show solid circles where the concentration of solute is 10% larger than the initial values, together with the output of Marlowe showing the location of displaced atoms at the end of the collisional phase.

This type of result is the main goal of this approach, as they can directly be related to what is observed in electron microscopy as cluster of defects after or during in situ irradiation. Clustering of solute atoms or intrinsic defects,

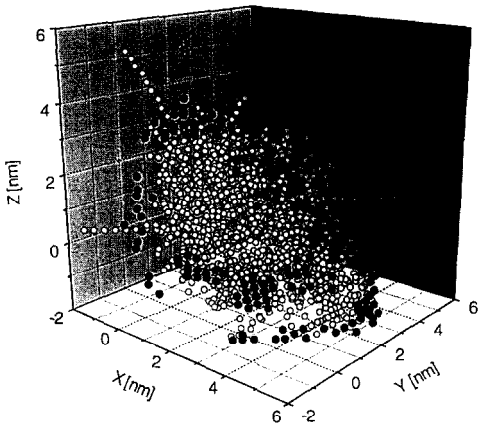

Fig. 5. Results for a 10 keV cascade in Ag as described by Marlowe and the liquid drop model, containing a low concentration of solute Cu. Open circles represent atoms that entered the cascade (output from Marlowe). Solid circles represent regions where the concentration of solute increased by more than 10%.

is the result of a very complex process and through this description some of the important components can quantitatively be accounted for. A detailed analysis of these preliminary results is on the way.

However, as mentioned earlier, the database from experiments is scarce for this temperature range, so here also, the computer simulations may provide valuable information. Solute diffusion in liquid metals as well as the coupling to thermal gradients c_T can be obtained from molecular dynamics in a straightforward way for some systems that can be easily modeled. As an example, we show in Fig. 7 self diffusion of liquid Ni, as calculated by the mean square displacement of a model system described in terms of the embedded atom model [17] with two sets of potential functions provided by the Sandia group, namely that for pure Ni and dilute transition metal impurities [18] and for Ni in the Ni–Al compound [19]. Also in Fig. 7 we

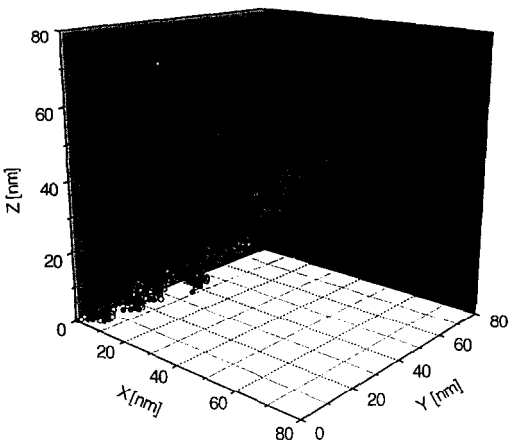

Fig. 6. As Fig. 5, for a 500 keV cascade in Ag.

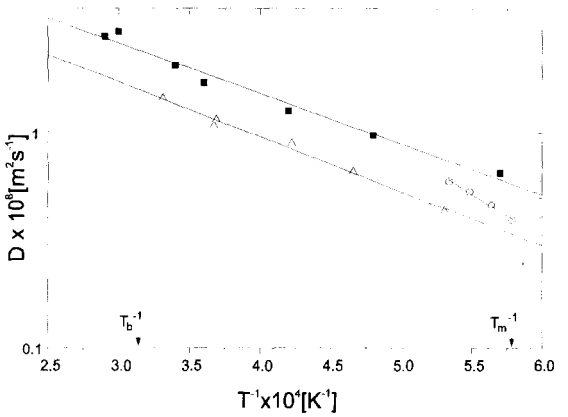

Fig. 7. Self diffusion of liquid Ni, using the embedded atom model with two sets of potential functions. Also shown results of a hard sphere model.

report the values predicted by Protopapas et al. [15] with their hard spheres model. As far as we are aware there is no experimental information for this metal. As we can see, Arrhenius plots correctly predicts the trends, but significant differences exists among the different description, revealing how difficult will be to arrive at a point where predictive capability in heat and mass transport in collision cascades be reached.

In summary, we show in this work some progress done in an analytic description of transport in collision cascades, namely a rigorous treatment of the 3D Stefan problem, a parametric study of mass transport in thermal gradients and preliminary results on a database for heat and mass transport in dilute metallic systems constructed using molecular dynamics simulations within the embedded atom model.

Although these effects produced by giant thermal gradients are probably the most relevant for the short term evolution of the microstructure, other factors, like thermodynamic forces derived from the phase diagram may also play a role in the picosecond time scale. Here also, computer simulations may help clarifying their relative importance.

References

[1] M. Caro, A. Ardelea, A. Caro, J. Mater. Res 5 (1990) 2657.
[2] M. Alurralde, A. Caro, M. Victoria, J. Nucl. Mater. 183 (1991) 33.
[3] M. Alurralde, A. Caro, M. Victoria, J. Mater. Res. 8 (1993) 449.
[4] M.T. Robinson, I.M. Torrens, Phys. Rev. B9 (1974) 5008.
[5] H. van Swygenhoven, A. Caro, Phys. Rev. Lett. 70 (1993) 2098.
[6] R.N. Nochetto, C. Verdi, SIAM J. 25 (1988) 784.
[7] R.N. Nochetto, in: Advances in Numerical Analysis (Oxford University, 1991).
[8] R.N. Nochetto, M. Paolini, C. Verdi, Mathemat. Comput. 57 (1991) 73.
[9] R.N. Nochetto, M. Paolini, C. Verdi, SIAM J. 12 (1991) 1207.
[10] F. Basombrio, in: Mecánica Computacional XVI, Asociación Argentina de Mecánica Computacional, Argentina, 1996.
[11] G. Strang, G. Fix, in: An Analysis of the Finite Element Methods (Prentice-Hall, Englewood Cliffs, 1973).
[12] L. Onsager, Phys. Rev. 37 (1931) 404.
[13] L. Onsager, Phys. Rev. 38 (1931) 2265.
[14] R. Kubo, M. Yokota, S. Nakajima, J. Phys. Soc. Jpn. 12 (1957) 1203.
[15] P. Protopapas, H.C. Andersen, N.A.D. Parlee, J. Chem. Phys. 59 (1973) 15.
[16] A. Sawatzxy, F.E. Jaunot, J. Met. 9 (1957).
[17] M.S. Daw, M.I. Baskes, Phys. Rev. Lett. 50 (1983) 1285.
[18] S. Foiles, M. Baskes, M.S. Daw, Phys. Rev. B33 (1986) 7983.
[19] S.M. Foiles, M.S. Daw, J. Mater. Res. 2 (1987) 5.